



**HAL**  
open science

## Numerical modelling of the suspended particulate matter dynamics in a regulated river network

M. Launay, V. Dugué, J.-B. Faure, Marina Coquery, B. Camenen, J. Le Coz

► **To cite this version:**

M. Launay, V. Dugué, J.-B. Faure, Marina Coquery, B. Camenen, et al.. Numerical modelling of the suspended particulate matter dynamics in a regulated river network. *Science of the Total Environment*, 2019, 665, pp.591-605. 10.1016/j.scitotenv.2019.02.015 . hal-02553064

**HAL Id: hal-02553064**

**<https://hal.science/hal-02553064>**

Submitted on 16 May 2020

**HAL** is a multi-disciplinary open access archive for the deposit and dissemination of scientific research documents, whether they are published or not. The documents may come from teaching and research institutions in France or abroad, or from public or private research centers.

L'archive ouverte pluridisciplinaire **HAL**, est destinée au dépôt et à la diffusion de documents scientifiques de niveau recherche, publiés ou non, émanant des établissements d'enseignement et de recherche français ou étrangers, des laboratoires publics ou privés.

## Numerical modelling of the suspended particulate matter dynamics in a regulated river network

M. Launay<sup>a,b</sup>, V. Dugué<sup>a,c</sup>, J.-B. Faure<sup>a</sup>, M. Coquery<sup>a</sup>, B. Camenen<sup>a</sup>,  
J. Le Coz<sup>a,1</sup>

<sup>a</sup>*Irstea, UR RiverLy, 5 rue de la Doua CS 20244, 69625 Villeurbanne Cedex, France*

<sup>b</sup>*Now at Stucky SA, Rue du Lac 33, 1020 Renens VD, Switzerland*

<sup>c</sup>*Now at CNR, Compagnie Nationale du Rhône, 2 rue André Bonin, 69004 Lyon, France*

---

### Abstract

Understanding and predicting the propagation, deposition and re-suspension of suspended particulate matter (SPM) in river networks is important for managing water resources, ecological habitat, pollution, navigation, hydropower generation, reservoir sedimentation, etc. Observational data are scarce and costly, and there is little feedback on the efficiency of numerical simulation tools for compensating the lack of data on a river scale of several hundreds of kilometres. This paper aims at exploring the use of a one-dimensional (1-D) hydrodynamical model for understanding the source and fate of SPM during complex events. The numerical model was applied to the May-June 2008 flood in the Lower Rhône River, France. This event was a combination of floods of the Isère (including dam flushing operations in the Lower Isère River) and Durance tributaries over a two-week period. The simulation code was used to model the SPM fluxes at a high spatial and temporal resolution using a multi-class approach. Approximately half of the 4.9 Mt of SPM measured at the outlet at Beaucaire were found to come from the Isère River and the other half from the Durance River, whereas previous studies estimated that most of the SPM flux at the outlet came from the Durance River. The amount of SPM trapped within the river network, mainly behind the first hydropower structure downstream of the Isère confluence, was estimated to be 3.7 Mt due to the deposition of the coarsest

---

\*Corresponding author

particles. Such a model proved to be able to compute the interaction of various grain size classes with dams and other structures. In turn, the quality of the results of SPM fluxes and deposition is highly sensitive to particle parameters, especially grain size distribution, and to the operational rules of reservoirs.

*Keywords:* suspended sediment, suspended solids, 1-D hydrodynamical model, numerical simulation, Rhône River, flood

---

## 1. Introduction

Monitoring the suspended particulate matter (SPM) dynamics in river systems is crucial for multiple environmental management issues, such as the ecological restoration of aquatic habitats, the sustainable operation of reservoirs, or the management of particle-bound contaminant fluxes (*Walling et al.*, 2003). These questions are generally facing a lack of data available at the watershed scale and at time scales from flood events to several years (*Horowitz et al.*, 2015). The presence of dams significantly affects the SPM dynamics with large deposition in the reservoirs and possible resuspension during specific events when dam gates are opened. Sediment management in dam reservoirs and regulated rivers is indeed one important issue of the 21st century (*Kondolf et al.*, 2014).

The development of station networks measuring SPM and particulate contaminants at large catchment scales remains limited due to the water sampling constraints and the cost of analyses (*Horowitz*, 2008). Data on SPM concentration ( $C_{\text{SPM}}$ ) are mostly derived from discrete water sampling carried out as part of water quality monitoring programs (*Walling and Webb*, 1985; *Phillips et al.*, 1999; *Horowitz et al.*, 2001). The frequency of these measurements, generally performed with a fixed periodicity, is almost never high enough to measure the fine temporal variations in  $C_{\text{SPM}}$ , leading to large uncertainties in flux budget estimation (*Moatar et al.*, 2008). In recent decades, the development of surrogate techniques (*Gray and Gartner*, 2010) such as Optical Backscatter Systems (OBS, also known as turbidity meters) has allowed the continuous measurement of the SPM concentration, provided that sufficient calibration data are available

24 (*Foster et al.*, 1992; *Gippel*, 1995; *Clifford et al.*, 1995; *Thollet et al.*, 2013; *Dru-*  
25 *ine et al.*, 2018). Hydro-sedimentary stations based on water sampling and/or  
26 turbidity measurements at one point of the cross-section rely on the assumption  
27 of homogeneous SPM concentration (*Horowitz*, 2008). Nevertheless, the direct  
28 measurement of  $C_{\text{SPM}}$  at the river basin scale remains very expensive, time con-  
29 suming and in many instances problematic, especially in inaccessible sections  
30 and during floods (*Ulke et al.*, 2017). Most of the time, field data are available  
31 only for a particular event or over a limited period of time (*Mano et al.*, 2008;  
32 *Navratil et al.*, 2012).

33 Together with the deployment of denser measuring networks, hydro-sedimen-  
34 tary modelling allows the development of operational tools to improve the knowl-  
35 edge of the fate of suspended sediment in the river network (*Wu et al.*, 2004).  
36 Moreover, it allows testing alternative management scenarios and several hy-  
37 potheses on the water and SPM inputs. The use of numerical hydro-sedimentary  
38 models has increased considerably in the last decades in conjunction with the  
39 advances in computational techniques. One-dimensional (1-D) codes are admit-  
40 ted to be suitable for simulation over large temporal and spatial scales as they  
41 require less field data and computational resources than 2-D and 3-D codes do.  
42 The limited ability of 1-D codes to reproduce fine physical processes is compen-  
43 sated by the stability of their numerical schemes and their fast calculation speed  
44 (*Papanicolaou et al.*, 2008; *El Kadi Abderrezzak and Paquier*, 2009). Numerous  
45 1-D codes have been developed and are frequently used for engineering pur-  
46 poses. Amongst others, *Wu et al.* (2004) and *Papanicolaou et al.* (2008) listed  
47 several 1-D codes and their applications to rivers and dam reservoirs. These  
48 codes can be classified according to their range of application or their formu-  
49 lations: steady/unsteady flow, fully coupled/semi-coupled/decoupled flow and  
50 suspended sediment modelling, uniform/non-uniform grain size, equilibrium/non-  
51 equilibrium suspended sediment transport model. 1-D modelling is particularly  
52 suitable for calculating SPM dynamics since SPM concentrations are generally  
53 assumed to be homogeneously distributed throughout a river cross-section and  
54 modelling transverse mixing is not necessary (*Garneau et al.*, 2015). Modelling

55 a flood event at the river basin scale requires i) calibrating the hydraulic and  
56 suspended sediment transport parameters, ii) specifying the water and SPM  
57 inputs (upstream boundary conditions) and iii) validating the results along the  
58 river system, including at the outlet.

59 The objective of this paper is to explore the use of a 1-D numerical model  
60 to better understand the spatial and temporal dynamics of SPM during floods  
61 throughout complex river networks. In particular, we test the application of  
62 a 1-D numerical model in simulating the SPM dynamics in a river regulated  
63 by a series of run-of-the-river dams and other infrastructure. There is indeed  
64 very limited feedback in the literature on the following questions. What kind of  
65 results is a 1-D model able to provide and what is the added value compared to  
66 observational data? What are the most sensitive parameters, hence the main  
67 sources of error? What are the most restrictive assumptions and the main  
68 perspectives for improvement?

69 The first part of the paper describes the May-June 2008 flood event in the  
70 Lower Rhône River. This hydro-sedimentary event was selected for testing the  
71 model as it was a typical combination of floods and dam flushing operations and  
72 it comes with a complete set of high temporal resolution measurements on the  
73 main tributaries and at the outlet. The second part of the paper presents the  
74 hydro-sedimentary numerical tools and the Rhône 1-D model used to simulate  
75 the May-June 2008 event. The Rhône 1-D model was developed as part of the  
76 Rhône Sediment Observatory (OSR) to become an efficient tool for managing  
77 SPM at the scale of the river basin. The third part details the results of the  
78 modelling and highlights the impacts of grain size distribution and hydropower  
79 structures on the simulated SPM concentrations and deposits. The main lessons  
80 learnt from the modelling exercise are briefly discussed and summarised in con-  
81 clusive comments.

## 82 2. Case study

### 83 2.1. The Rhône River

84 The Rhône River flows 810 km from its source in the Swiss Alps to its out-  
85 let to the Mediterranean Sea in the South of France (Fig. 1). It is the largest  
86 single source of freshwater to the Mediterranean Sea (*Ludwig et al.*, 2009). Its  
87 hydrological regime is influenced by snow melting in headwater catchments,  
88 and by oceanic and Mediterranean rain events (*Pardé*, 1925). The three tribu-  
89 taries with the largest mean discharges are the Saône, Isère and Durance Rivers  
90 (Tab. 1). The Rhône River basin is characterized by a large geological and  
91 climatic heterogeneity, and by a dense network of hydropower schemes. From  
92 Lake Geneva to the Mediterranean Sea, the Rhône River is equipped with 21  
93 hydropower schemes, all of which are run-of-the-river schemes except Génissiat  
94 Dam in the Upper French Rhône River (Fig. 1).

95 The Bourg-lès-Valence scheme detailed in Fig. 1 is typical of the other run-of-  
96 the-river, by-passing hydropower plants (cf. *Camenen et al.* (2019) for a detailed  
97 description and analysis of sand fluxes). The Roche-de-Glun dam controls the  
98 discharge distribution between the Old Rhône and the power canal containing  
99 the Bourg-lès-Valence hydropower plant. A minimum compensation discharge  
100 is maintained in the Old Rhône at any time. During floods, when discharge  
101 exceeds the canal capacity, the excess flow is released in the Old Rhône. The  
102 particularity of this scheme lies in the confluence between the Isère River and  
103 the canal. In case of flood of the Isère River, the so-called Isère dam located  
104 between the headrace canal and the Old Rhône (cf. Fig. 1) can derive the excess  
105 discharge into the Old Rhône.

106 The Rhône River delivers substantial amounts of SPM to the Mediterranean  
107 Sea (*Radakovitch et al.*, 2008; *Launay*, 2014) with a mean inter-annual SPM  
108 flux varying between 4.7 and 7.4 Mt/yr (*Pont et al.*, 2002; *Eyrolle et al.*, 2012;  
109 *Ollivier et al.*, 2010; *Launay*, 2014; *Copard et al.*, 2018; *Poulier et al.*, 2019)  
110 but with huge variations of the annual SPM flux from one year to another. For  
111 example, annual SPM flux ranged from 1.2 to 22.7 Mt/yr between 1992 and

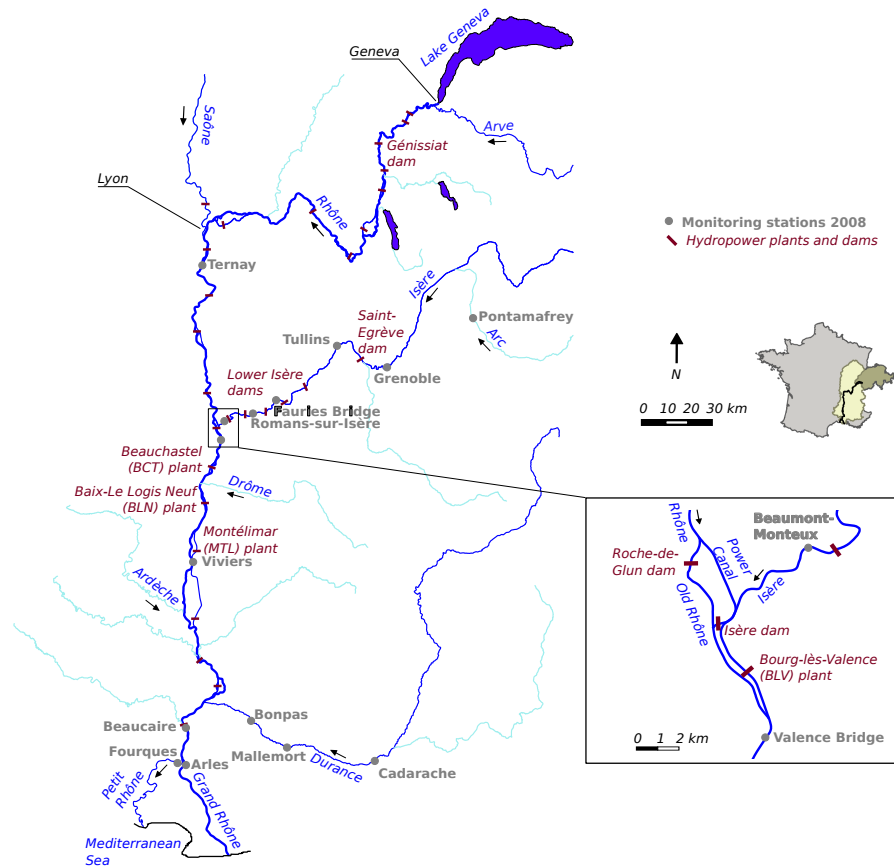


Figure 1: River network and hydroelectric schemes of the Rhône River from Lake Geneva to the Mediterranean Sea with a close-up view of the Bourg-lès-Valence hydroelectric scheme at the Rhône-Isère confluence. Monitoring stations of the May-June 2008 flood event in the Rhône, Arc, Isère and Durance Rivers are displayed.

112 1995 (*Pont, 1997*). Based on the long-term monitoring of  $C_{SPM}$  at Arles near  
 113 the delta of the Rhône River, *Eyrolle et al. (2012)* showed that singular events  
 114 (flood or dam flushing) can represent up to 95 % of the annual SPM budget. The  
 115 need for a better monitoring of SPM fluxes through the Rhône River motivated  
 116 the creation of the Rhône Sediment Observatory (OSR) in 2009. As part of the  
 117 OSR, an SPM monitoring network in the Rhône River and its tributaries from  
 118 Lake Geneva to the Mediterranean Sea was developed mostly based on turbidity  
 119 measurements calibrated with frequent SPM samples.

Table 1: General information on the catchments and hydrological regimes of the Rhône River and its main tributaries.

Station	$A$ [km <sup>2</sup> ]	$Q_a$ [m <sup>3</sup> /s]	$F_a$ [Mt/yr]	$Q_{max,2003}$ [m <sup>3</sup> /s]	$Q_{max,2008}$ [m <sup>3</sup> /s]	$C_{max,2008}$ [g/L]
Rhône at Lyon	20 300	600	0.6	813	1 206	-
Saône at Lyon	29 908	475	0.4	1 262	568	-
Isère at Beaumont	11 890	333	2.3	1 513	1 458	25.2
Durance at Bonpas	14 225	190	1.7	1 496	1 495	11.1
Rhône at Beaucaire	95 590	1 690	4.7-6.7	11 500	5 126	5.0

$A$  = catchment area,  $Q_a$  = mean annual discharge,  $F_a$  = mean annual SPM flux according to *Launay* (2014),  $Q_{max,2003}$  and  $Q_{max,2008}$  = maximum discharges for the events of December 2003 and May-June 2008,  $C_{max,2008}$  = maximum  $C_{SPM}$  for the May-June 2008 flood event.

120 According to *Launay* (2014) and *Poulier et al.* (2019), the main four tribu-  
 121 taries in terms of SPM contribution to the Rhône River are the Arve River, the  
 122 Saône River, the Isère River and the Durance River (Fig. 1 and Tab. 1). The  
 123 SPM output of Lake Geneva is assumed to be negligible due to the large trap-  
 124 ping capacity of the lake. The Isère and Durance Rivers are left bank alpine  
 125 tributaries of the Rhône River with fast and violent floods. The main SPM  
 126 contributor of the Isère River is the Arc River, a mountainous river producing  
 127 fine SPM (*Camenen et al.*, 2016). The six Lower Isère dams located between  
 128 Grenoble and the Rhône confluence near Valence (Fig. 1) are run-of-the-river  
 129 dams. Only the lowest Isère dam, Beaumont-Montoux, by-passes the Isère River  
 130 with a derivation canal.

### 131 2.2. The 2008 hydro-sedimentary flood event

132 In May-June 2008, a major hydro-sedimentary event occurred in the Lower  
 133 Rhône River, combining natural floods in its two main tributaries, the Isère



134 and Durance Rivers, and flushing operations of the Lower Isère dams. All the  
135 reservoirs of the Lower Isère and the Lower Rhône are run-of-river dams with  
136 very limited storage capacity. They can be partially drained and sediment  
137 flushing operations must meet precise regulation requirements. Isère dams can  
138 be flushed during flood falling phases in order to evacuate excess deposited  
139 sediment. Rhône dams are not expected to be flushed but their operation can  
140 be adapted to avoid deposition in critical areas such as around navigation locks  
141 or dam gates. This could not be done during the 2008 event presented here due  
142 to a lack of understanding and forecasting of the hydro-sedimentary processes,  
143 and a lack of real-time coordination between the two distinct companies that  
144 operate the Isère dams and the Rhône dams, respectively.

145 The peak discharge recorded at the Beaucaire station during this event was  
146  $5\,125\text{ m}^3/\text{s}$ , corresponding to a 2-year return period flood. Between May 26th  
147 and June 8th 2008, the Arles station recorded a total SPM flux of 4.2 Mt at the  
148 Rhône outlet (*Eyrolle et al.*, 2012), equivalent to the SPM output of the 100-year  
149 flood in 2003 which had a twice larger peak discharge (Tab. 1). The May-June  
150 2008 flood event in the Lower Rhône River was also remarkable because it  
151 produced an SPM flux almost equal to the mean annual SPM export of the  
152 Rhône River to the Mediterranean Sea recorded since 2005 (*Launay*, 2014).

153 During the 2008 flood event, SPM concentrations were measured at the  
154 monitoring stations presented in Fig. 1, either continuously using OBS or the  
155 acoustic attenuation method presented by *Moore et al.* (2012), or by sampling-  
156 filtration method (*AFNOR*, 2005). All the SPM samples were taken near the  
157 free-surface using buckets or automatic samplers. They include the homoge-  
158 neously distributed suspension ("washload"), not the graded sand suspension.  
159 Well mixed cross-sections were chosen for the monitoring of  $C_{\text{SPM}}$  except for  
160 the Rhône station at Valence Bridge, where the Isère and Rhône waters were  
161 not fully mixed. Available SPM data cover the Arc-Isère-Rhône river network,  
162 the Rhône-Isère confluence with numerous samples, the Durance River network,  
163 and some stations along the Rhône River.

164 Fig. 2 presents the water discharge times series and  $C_{\text{SPM}}$  data collected

165 during the event at the outlet of the Arc, Isère and Durance Rivers, and at four  
166 stations of the Rhône River. The Rhône at Ternay station is located upstream of  
167 the Isère confluence and monitors the discharge and SPM inputs from the Upper  
168 Rhône River. The Rhône at Viviers station provides an intermediate checkpoint  
169 to study the Isère River input independently from the Durance input. This is  
170 the first monitoring station downstream of the Isère confluence with a complete  
171  $C_{\text{SPM}}$  time series for the May-June 2008 flood event, while the Rhône at Valence  
172 station recorded  $C_{\text{SPM}}$  only during the third period of the event. The Beaucaire  
173 station located near the outlet of the Rhône River gives indication on the SPM  
174 fluxes delivered to the Mediterranean Sea. The Beaucaire station is the last  
175 discharge monitoring station for the Rhône River before the separation of the  
176 two branches of the Rhône Delta. The measurement of  $C_{\text{SPM}}$  is performed at  
177 the Arles station located about 13 km downstream on the Grand Rhône branch.  
178 The SPM concentrations are considered to be the same at Beaucaire and Arles  
179 for the SPM flux calculation.

180 The measured SPM fluxes were determined by multiplying the instanta-  
181 neous water discharges and the instantaneous  $C_{\text{SPM}}$ . For monitoring stations  
182 with occasional  $C_{\text{SPM}}$  measurements (samples), the SPM fluxes were estimated  
183 by establishing a power relation between discharge and  $C_{\text{SPM}}$  to reconstruct a  
184 continuous  $C_{\text{SPM}}$  time series.

185 The event can be divided into three SPM-producing periods (Fig. 2). The  
186 first period covers the dam flushing of the Saint-Egrève dam occurring between  
187 26/05/2008 and 29/05/2008 in the Isère River. This dam flushing was trig-  
188 gered concomitantly with a 1-year return period flood of the Isère River, with  
189 discharges up to 1 000 m<sup>3</sup>/s at the Beaumont-Montoux station. During this pe-  
190 riod, the Lower Isère dams were operated with high water levels in the reservoirs,  
191 and the water overflowing the gates. Meanwhile, a substantial flood occurred  
192 in the Durance River, with  $C_{\text{SPM}}$  greater than 10 g/L on the 27/05/2008. The  
193 management of the hydropower schemes of the Durance River during this pe-  
194 riod led to mitigate the discharge (around 800 m<sup>3</sup>/s) while releasing a large  
195 amount of SPM. To account for the flood wave time lag between the upstream

196 part of the catchment and its downstream part, the ending date of the first  
197 period was postponed to the 30/05/2008 for the downstream part. During the  
198 second period, from 29/05/2008 to 02/06/2008, a large flood of the Arc River  
199 was recorded with  $C_{\text{SPM}}$  greater than 30 g/L, causing a  $C_{\text{SPM}}$  peak greater  
200 than 20 g/L in the Isère at Beaumont-Monteux on the 30/05/2008. This peak  
201 propagated in the Rhône River and about 8 g/L were recorded at Viviers on  
202 the 31/05/2008. During this period, the Lower Isère dams were not flushed,  
203 but the bottom gates were opened. The second period runs from 30/05/2008  
204 to 03/06/2008 to account for flood propagation delay. During this period, a  
205 major flood occurred in the Durance River with discharge up to 1 500 m<sup>3</sup>/s and  
206  $C_{\text{SPM}}$  up to 6 g/L. The third period lasted from 02/06/2008 to 10/06/2008, for  
207 which the Lower Isère dams were flushed, with low water level in the reservoirs  
208 to evacuate the deposited sediments. The cloud of SPM was recorded around  
209 04/06/2008 in the Isère at Beaumont-Monteux with maximum  $C_{\text{SPM}}$  around  
210 20 g/L. It was recorded in the Rhône at Viviers with a propagation delay of one  
211 day and the peak  $C_{\text{SPM}}$  was about 2 g/L.

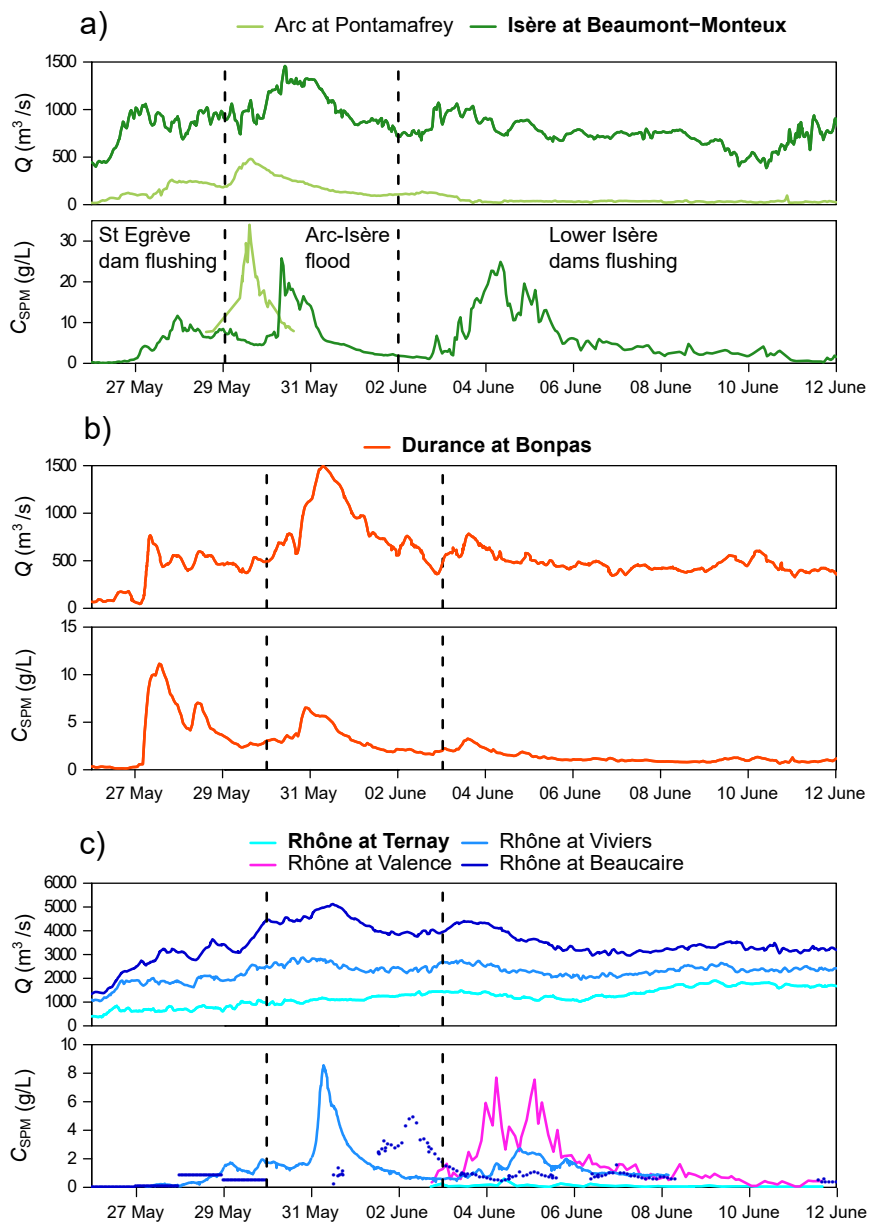


Figure 2: Discharges and SPM concentration ( $C_{\text{SPM}}$ ) in (a) the Arc and Isère Rivers, (b) the Durance River and (c) the Rhône River during the May-June 2008 flood event. The limits of the three periods are shown with vertical dashed lines: on the 29/05/2008 and 02/06/2008 for the Isère River, on the 30/05/2008 and 03/06/2008 for the Durance River and the Lower Rhône River. Monitoring stations indicated in bold are the upstream boundary conditions of the model.

212 *2.3. SPM inputs from the Isère River*

213 A  $C_{\text{SPM}}$  time series was reconstructed at the outlet of the Isère River since  
214 a continuous  $C_{\text{SPM}}$  time series was not available at the Isère at Beaumont-  
215 Monteux for the entire event (Fig. 3). The measurements used for the re-  
216 construction were taken at Tullins (turbidimeter, *Rieux, 2008*), Romans-sur-  
217 Isère (side-looking hydroacoustic profiler, *Moore et al., 2012*), Beaumont-Mon-  
218 teux (manual water samples, *Rieux, 2008*) and the Rhône at Viviers. Between  
219 26/05/08 and 30/05/08, the reconstructed  $C_{\text{SPM}}$  time series followed the mea-  
220 surements at Romans-sur-Isère, the closest station upstream of Beaumont-Mon-  
221 teux, with an estimated time lag of 1 h. Time lag between stations was cal-  
222 culated based on  $C_{\text{SPM}}$  peaks. Similarly, between 01/06/08 and 02/06/08, the  
223 reconstructed  $C_{\text{SPM}}$  time series followed the measurements at Tullins with an  
224 estimated time lag of 10 h. However data based on Tullins station may be un-  
225 derestimated if erosion occurs in the Lower Isère reservoirs. Between 30/05/08  
226 and 01/06/08, those reservoirs were flushed; as no representative measurements  
227 were available, the SPM concentration at Beaumont-Monteux was evaluated as  
228 the SPM flux in the Rhône at Viviers divided by the water discharge of the Isère  
229 at Beaumont-Monteux. The rationale behind this computation is that during  
230 that period the SPM flux coming from the Rhône upstream of the Isère junction  
231 was negligible with respect to the SPM flux coming from the Isère. This ap-  
232 proximation is reasonable as discharges and SPM concentrations remained very  
233 low in the Rhône upstream of the Isère junction during that period of time.  
234 Finally, from 03/06/2008 on, SPM concentrations were measured at Beaumont-  
235 Monteux.

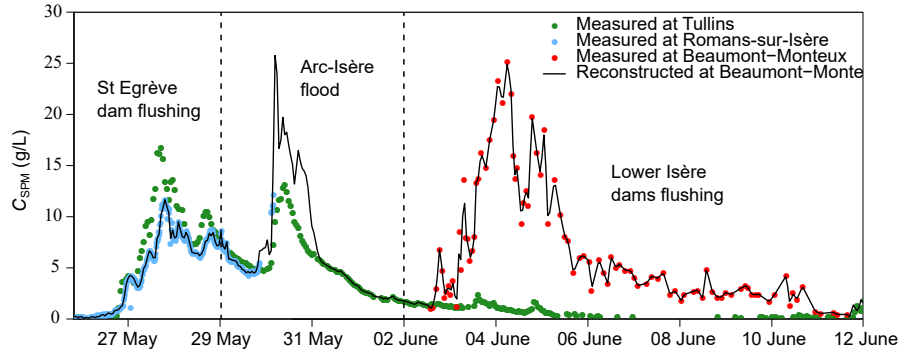


Figure 3: Reconstruction of the SPM concentration ( $C_{SPM}$ ) time series of the Isère River at Beaumont-Monteux station from SPM measurements at Tullins and Romans-sur-Isère stations from 26/05/2008 to 12/06/2008.

### 236 3. 1-D modelling of the May-June 2008 flood event

#### 237 3.1. Numerical codes

238 The 1-D hydro-sedimentary numerical tool used in this study was developed  
 239 by Irstea. It couples the Mage and AdisTS hydro-sedimentary numerical codes.  
 240 Mage (*Souhar and Faure, 2009*) is a 1-D hydrodynamic code which simulates  
 241 transient open-channel flows by solving the 1-D Barré de Saint-Venant equations  
 242 (shallow water equations):

$$\frac{\partial A_w}{\partial t} + \frac{\partial Q}{\partial x} = q_{lat} \quad (1)$$

$$\frac{\partial Q}{\partial t} + \frac{\partial}{\partial x} \left( \beta \frac{Q^2}{A_w} \right) + g A_w \frac{\partial z}{\partial x} = -gS(J + J_s) + k q_{lat} V \quad (2)$$

244 where  $A_w$  is the wetted area,  $Q$  the water discharge,  $t$  the time,  $x$  the lon-  
 245 gitudinal coordinate,  $q_{lat}$  a lateral input/output discharge,  $\beta$  the momentum  
 246 coefficient,  $z$  the water surface elevation,  $J$  the energy slope computed using  
 247 the Manning-Strickler equation,  $J_s$  the local energy losses due to sharp varia-  
 248 tion of the cross-section,  $k$  a coefficient depending on the sign of  $q_{lat}$  ( $k = 1$  if  
 249  $q_{lat} < 0$ ,  $k = 0$  if  $q_{lat} \geq 0$ ), and  $V = Q/A_w$  the cross-section-averaged velocity.

250 Mage describes the real geometry of the river bed as a series of cross-sections,  
 251 and accounts for compound channel effects using the Debord equations (*Nicollet*

252 and *Uan*, 1979). Storage nodes can be defined to model floodplain areas where  
 253 the water velocity may be assumed to be negligible. No storage nodes were used  
 254 in the presented simulations. The river network topology may be looped (bi-  
 255 furcations, confluences), with multiple downstream boundary conditions. The  
 256 1-D Barré de Saint-Venant equations are solved using a four point semi-implicit  
 257 finite-difference scheme (Preissmann scheme).

258 AdisTS (*Guertault et al.*, 2016) is a 1-D code solving mass conservation  
 259 equations for SPM transport in parallel. The code includes advection-dispersion  
 260 equations in conservative formulation (Eq. 3) for several SPM classes. SPM  
 261 grain size distribution (GSD) is reproduced by mixing a fixed number of classes  
 262 of different proportion. The equations are coupled using source terms that allow  
 263 modelling erosion and deposition terms:

$$\frac{\partial A_w C_i}{\partial t} + \frac{\partial Q C_i}{\partial x} - \frac{\partial}{\partial x} \left( D_f A_w \frac{\partial C_i}{\partial x} \right) = (E_i - D_i) W_z \quad (3)$$

264 where  $C_i$  is the concentration in SPM class  $i$ ,  $E_i$  and  $D_i$  are erosion and depo-  
 265 sition fluxes of SPM class  $i$ ,  $D_f$  is the longitudinal diffusion coefficient, and  $W_z$   
 266 is the river width. The source term combines the *Partheniades* (1965) formula  
 267 for erosion and the *Krone* (1962) formula for deposition:

$$E_i - D_i = a_{PD,i} (C_{eq,i} - C_i) w_{s,i} \quad (4)$$

268 where  $C_{eq,i}$  is the equilibrium concentration for the SPM class  $i$ ,  $a_{PD,i}$  is a  
 269 recovery coefficient, reflecting non equilibrium sediment transport (*Han*, 1980;  
 270 *Armanini and Di Silvio*, 1988), and  $w_{s,i}$  is the settling velocity of the SPM class  
 271  $i$ . The equilibrium concentration depends on the effective bed shear stress,  $\tau_{eff}$   
 272 as:

$$C_{eq,i} = \begin{cases} C_{0,i} \left( \frac{\tau_{eff}}{\tau_{cr,i}} - 1 \right) & \text{if } \frac{\tau_{eff}}{\tau_{cr,i}} > 1 \\ 0 & \text{otherwise} \end{cases} \quad (5)$$

273 where  $C_{0,i}$  is a calibration concentration specific to SPM class  $i$ ,  $\tau_{cr,i}$  is the  
 274 critical shear stress for initiation of movement of SPM class  $i$ , estimated using  
 275 the Shields diagram. For fine sediments ( $d < 70 \mu\text{m}$ ), since consolidation can  
 276 be neglected when simulation is performed at event scale, the critical bed shear

277 stress is assumed independent of the grain size for fine sediments ( $\tau_{cr} = 0.15$  Pa).  
278 The effective bed shear stress is computed as  $\tau_{eff} = (K_S/K'_S)\tau$ , with  $K_S$  the  
279 total Strickler coefficient,  $K'_S = 24/d_{90}^{1/6}$  the skin-friction Strickler coefficient.  
280 The total bed shear stress  $\tau = \rho g R_h J$  is computed using the 1-D hydraulic  
281 model ( $\rho$  water density and  $R_h$  hydraulic radius). The calibration of the two  
282 AdisTS parameters,  $a_{PD,i}$  and  $C_{0,i}$ , was performed as functions of the grain size  
283 by *Guertault et al.* (2016) on Génissiat hydropower scheme in the Rhône River.

284 The longitudinal diffusion coefficient  $D_f$  was calculated using the formula of  
285 *Iwasa and Aya* (1991) as *Launay et al.* (2015) concluded it was the best suited  
286 based on their analysis of tracing experiments and hydro-acoustic measurements  
287 in the Rhône River near Lyon.

288 AdisTS is loosely coupled with Mage software. The bed geometry remains  
289 fixed over time but the model simulates a potential stock of sediments available  
290 over each channel (main channel and floodway) in each cross-section. This stock  
291 is spatially distributed using a mean thickness and assuming a constant porosity  
292  $p = 0.45$ ; it can vary in mass and GSD over time due to erosion and deposition.  
293 Indeed, the advection-dispersion equation is solved for each sediment class and  
294 the GSD of bed sediment stocks depend on the erosion or deposition simulated  
295 along the system for each class independently. It is possible to specify initial  
296 sediment stocks along the river system but for the presented simulations no ini-  
297 tial stock was assumed. Over long timescales, there may be geometric feedbacks  
298 that change channel capacity when erosion and sedimentation do not balance.  
299 However, the fixed-bed assumption has limited consequences over the timescale  
300 of an individual event. It allows a faster calculation which is of particular inter-  
301 est when dealing with long river reaches and long-term scenarios with limited  
302 bed evolution.

303 The 1-D numerical tool can be used to identify the origin of the water flowing  
304 at a downstream monitoring station. This identification is done by injecting a  
305 numerical tracer in each tributary  $j$  with concentration  $C_{j,ref} = 1$  g/L. At a  
306 downstream monitoring station where the total water discharge  $Q$  is calculated,  
307 the proportion of water  $Q_j/Q$  coming from the tributary  $j$  can be determined



308 based on the tracer mass continuity equation:  $Q_j/Q = C_j/C_{j,\text{ref}}$ , where  $C_j$   
309 is the concentration of tracer coming from the tributary  $j$  calculated at the  
310 station. Similarly, each SPM class  $i$  from each tributary  $j$  can be traced so  
311 that concentration  $C_{\text{SPM},i,j}$  is computed at each node and at each time of the  
312 simulation.

### 313 3.2. 1-D model of the Rhône River

314 The Rhône 1-D model, developed by Irstea as part of the OSR program, rep-  
315 represents the Rhône River from Lake Geneva to the Mediterranean Sea (Fig. 1).  
316 Bathymetry surveys of the river cross-sections are available every 500 m stream-  
317 wise. Lidar data were used to complete some profiles in the main channel and  
318 to estimate the extent of the floodway. Additional profiles were included to rep-  
319 resent dams and hydroelectric plants. In the model, cross-sectional profiles were  
320 interpolated every 100 m. Cross-sections of the major tributaries (Arve, Ain,  
321 Saône, Isère and Durance Rivers) were also included to represent their lowest  
322 sections up to their confluences with the Rhône River. Other tributaries are  
323 only represented as local inputs.

324 Flow resistance coefficients of the main channel ( $30 \leq K_S \leq 42 \text{ m}^{1/3}/\text{s}$ )  
325 were calibrated and validated over each reach using longitudinal water profiles  
326 measured over a wide range of discharges from low water to flood conditions  
327 ( $1500 \leq Q \leq 4500 \text{ m}^3/\text{s}$ ). It was not necessary to vary the flow resistance  
328 coefficients with discharge to achieve an acceptable calibration, i.e. stage errors  
329 lower than 0.1 m, typically. Flow resistance coefficients of the floodways (over  
330 bars, islands, etc.) were assumed to be equal to  $20 \text{ m}^{1/3}/\text{s}$  everywhere. The  
331 floodways of the Rhône River are narrow due to the presence of dykes and  
332 overbank flows are limited. Therefore, the results are not much sensitive to the  
333 values of the flow resistance coefficient defined for the floodways. The model  
334 does not include floodplains and cannot be used to simulate flooding over dikes.

335 The model includes the operation rules of the 21 run-of-the-river hydropower  
336 schemes (Dugué *et al.*, 2015). All the Rhône dams included in the model have  
337 a bypass channel (remember that no Isère dams are included in the computa-

338 tional domain). The operation rules of the run-of-the-river hydropower schemes  
339 impose a minimum compensation discharge in the bypassed channel and a max-  
340 imum discharge in the power canal as allowed by the hydropower plant (*Dugué*  
341 *et al.*, 2015). Also, the maximum water level at a regulation point in each reser-  
342 voir is prescribed through legal dam operation rules which the operator has to  
343 follow, especially during floods, whatever the initial storage is. Such run-of-  
344 river dams actually have a limited storage capacity and the water level in the  
345 reservoir can be regulated by opening the dam gates, typically. The legal dam  
346 operation rules are specific to each dam and relate the maximum allowed water  
347 level as a function of inflow, usually.

348 For the specific study of the May-June 2008 flood event, the 1-D numerical  
349 model was restricted to the Lower Rhône River, starting from Ternay station.  
350 Eleven hydropower schemes are present in the study area. In this configuration,  
351 the model has three main upstream boundary conditions: the Rhône at Ternay,  
352 the Isère at Beaumont-Monteux (i.e. just downstream of the last dam of the  
353 Lower-Isère chain of dams) and the Durance at Bonpas (see Fig. 1). The smaller  
354 tributaries located between Ternay and the Mediterranean Sea are considered  
355 as local water inputs. Both discharge and  $C_{\text{SPM}}$  time series for the three main  
356 upstream boundaries are indicated as thick lines in Fig. 2. The discharge of the  
357 smaller tributaries were also simulated. The downstream boundary conditions  
358 on the Rhône Delta are the water levels measured in the Grand Rhône branch  
359 and in the Petit Rhône branch (cf. Fig. 1).

360 Upstream of the Isère confluence, the SPM concentration in the Rhône River  
361 at Ternay was lower than 0.2 g/L typically (cf. Fig. 2c), which is much lower  
362 than the SPM concentration of the Isère and Durance tributaries during the  
363 flood event. As the discharge time series at Ternay does not indicate any flood,  
364 the SPM input at Ternay was set to zero for the simulations. The  $C_{\text{SPM}}$  time  
365 series used as input for the Isère River at Beaumont-Monteux was reconstructed  
366 as discussed in section 2.3. For the Durance River, SPM time series was recorded  
367 at Bonpas turbidity station (Fig. 2b). SPM inputs from smaller tributaries were  
368 considered to be negligible during the May-June 2008 flood event compared to

369 the inputs of the Isère and Durance Rivers.

### 370 3.3. Grain size distributions

371 The 1-D numerical model requires information on the grain size distribution  
372 (GSD) of the SPM. Numerical simulations on the Rhône River were performed  
373 using six SPM classes with variable grain sizes from clay to medium sand, and  
374 assuming grain size distribution of each class to be log-normal of parameters  
375  $d_{50,i}$  and  $\sigma_i$  (see Tab 2).  $d_{50,i}$  and  $\sigma_i$  are assumed constant in time; only the  
376 relative proportion of the class  $i$  (in the total SPM concentrations and stocks)  
377 may vary in time.

378 The three classes with the finest SPM were determined based on grain size  
379 analysis of Rhône SPM samples (Launay, 2014) and the three classes with the  
380 coarsest SPM were defined by Guertault (2015). These classes were defined  
381 so as to best represent main groups of particles that systematically show up  
382 in the measured grain size distributions. Eventually, only the first four finest  
383 classes will be used for this study, the two coarsest sand classes being easily  
384 trapped by dam reservoirs (Camenen *et al.*, 2019). The representative settling  
385 velocity  $w_{s,i}$  for each class of sediment  $i$  was calculated using Camenen (2007)  
386 formula and assuming the grain size distribution of each class to be log-normal  
387 (cf. Tab. 2). Cohesion is neglected since organic content is very low ( $< 5\%$ ,  
388 typically) as well as cohesiveness (Legout *et al.*, 2018). The impact on settling  
389 velocity (flocculation) is thus relatively low, and there is actually no possible  
390 validation of any flocculation model for this specific case.

391 No GSD was measured in the Isère or Durance Rivers during the May-June  
392 2008 flood event. Grain size analysis of the SPM of the Isère River in 2008 and  
393 during a similar hydrological event in 2015 showed that the particles of the Isère  
394 River and the SPM collected in the Rhône River during the 2012 dam flushes  
395 have similar grain size distributions. Therefore, the parameters calibrated by  
396 Guertault *et al.* (2016) were kept to simulate the 2008 flood event. The same  
397 assumption was made on Durance SPM although no grain size analysis was  
398 performed on SPM samples of the Durance River.

Table 2: Physical properties of the elementary SPM classes and AdisTS coefficients  $a_{PD,i}$  and  $C_{0,i}$ , as proposed by Guertault (2015). Proportions of the SPM classes in the three SPM mixtures tested with the numerical model for the Isère input.

Name	Class 1	Class 2	Class 3	Class 4	Class 5	Class 6
Median diameter: $d_{50,i}$ ( $\mu\text{m}$ )	4	15	45	90	200	400
Standard deviation of $\ln(d_i)$ : $\sigma_i$ (-)	0.32	0.24	0.17	0.17	0.20	0.20
Settling velocity: $w_{s,i}$ (m/s)	$2.8 \cdot 10^{-5}$	$2.3 \cdot 10^{-4}$	$1.4 \cdot 10^{-3}$	$7.5 \cdot 10^{-3}$	$2.6 \cdot 10^{-2}$	$5.8 \cdot 10^{-2}$
Critical shear stress: $\tau_{cr,i}$ (Pa)	0.153	0.154	0.155	0.158	0.174	0.232
Recovery coefficient: $a_{PD,i}$	1	1	1	1	1	1
Calibration concentration: $C_{0,i}$ (g/L)	1	1	0.5	0.2	0.2	0.2
% in Mixture A - Fine	31	44	25	0	0	0
% in Mixture B - Medium	23	28	31	18	0	0
% in Mixture C - Coarse	12	18	40	30	0	0

399 Samples collected in other occasions in the Arc-Isère network were used to  
400 determine three possible GSD for the SPM transported by the Isère River in  
401 May-June 2008, named Mixtures A, B and C (see Fig. 4 and Tab. 2). The  
402 measured GSD were approximated using a mixture of log-normal distributions,  
403 as explained by Masson *et al.* (2018).

404 Two surface water samples were collected during floods of the Arc River  
405 (June 2015, documented by Camenen *et al.* (2016)) and the Isère River (May  
406 2015). The Arc River is the main natural SPM input to the Isère River. The  
407 SPM usually transported by the Arc River represent the finest SPM transported  
408 during a flood in the Arc-Isère river network (classes 1 and 2 composed of clay  
409 and fine silt). They were averaged to give Mixture A - Fine GSD (Fig. 4).  
410 Two samples of riverbed sediment were collected in the Rhône River after the  
411 May-June 2008 flood event. One sample was collected downstream of the Bourg-  
412 lès-Valence (BLV) plant (06/08/2008), and the other sample was collected in  
413 the garage of the BLV lock (23/06/2008). Additionally, one sample was taken  
414 after the flood of May 2015 from a deposit near the right bank of the Isère  
415 River downstream of Beaumont-Montoux. Bank deposit and riverbed sediment

416 samples correspond to the coarsest SPM transported during a flood. They were  
417 averaged to compose Mixture C - Coarse GSD, which is considered as an extreme  
418 scenario for which most of the SPM would be made of that coarsest fraction.  
419 Finally, one sample taken in the water column close to the bottom at the Rhône  
420 and Isère confluence during the May 2015 flood contained particles from clay to  
421 coarse silt in equal proportions. This intermediate sample constitutes Mixture  
422 B - Medium GSD.

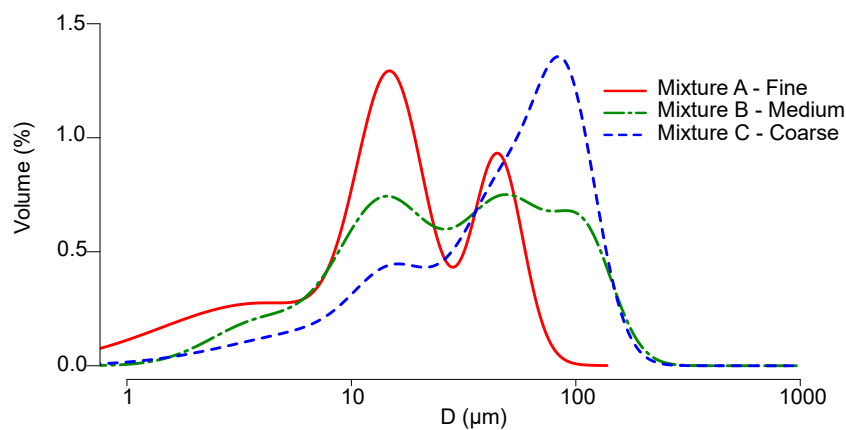


Figure 4: Three possible grain size distributions for the SPM transported by the Isère River during the May-June 2008 flood event.

423 The SPM of the Durance River was assumed to be composed of clay only  
424 (class 1), with a median diameter  $d_{50}$  of 4  $\mu\text{m}$ . This hypothesis relies only  
425 on field observation of the very fine aspect of the washload transported by the  
426 Durance River.

## 427 4. Results

### 428 4.1. Origin of water discharge during the May-June 2008 flood event

429 The contributions of the Isère and Durance Rivers to the Rhône River water  
430 discharge during the May-June 2008 event were evaluated using the 1-D model.  
431 The hydrograph decomposition results are presented for the Rhône at Valence

432 Bridge, Viviers and Beaucaire stations (Fig. 5). Overall, the simulated discharge  
433 is within 10% of the measured discharge, except for short transient phases. This  
434 is less than the expected level of uncertainty of hourly discharge measurements  
435 (Horner *et al.*, 2018), which suggests that the main sources of water and their  
436 propagation through the river network are correctly simulated by the model.

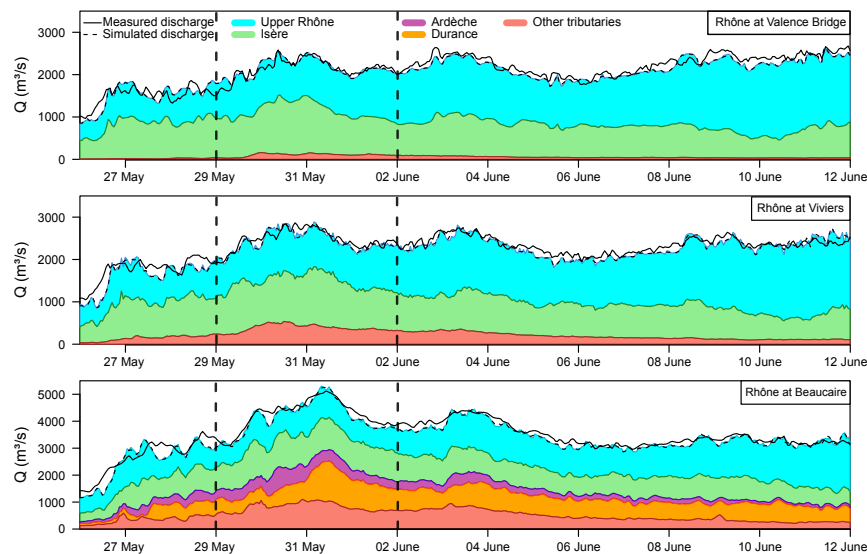


Figure 5: Decomposition of the flow hydrographs of the May-June 2008 flood event at the hydrometric stations of the Rhône at Valence, Viviers and Beaucaire using the 1-D hydrodynamic model. The three periods (see section 2.2) are separated by the vertical dashed lines.

437 At Valence Bridge station (Fig. 5a), two water sources can be distinguished:  
438 the Upper Rhône River (upstream of Ternay) and the Isère River. The contri-  
439 bution of the tributaries between Ternay and Valence was very small during the  
440 event. The Upper Rhône River was not in flood during the period of the May-  
441 June 2008 flood event, so the shape of the hydrograph at Valence Bridge was  
442 mainly influenced by the Isère River contribution. At Viviers station (Fig. 5b),  
443 the contribution of the tributaries other than the Isère is increased by water  
444 inputs from the Eyrieux, Drôme, Right-bank Ouvèze and Roubion Rivers. The

445 discharge contribution of these tributaries is higher than that of previous trib-  
446 utaries between Ternay and Valence but remains small. At Beaucaire (Fig. 5c),  
447 most of the water came from the Upper Rhône (from 20 to 40 %), the Isère  
448 (around 25 %) and the Durance (around 25 %) Rivers, with smaller inputs from  
449 the Ardèche and other tributaries.

#### 450 4.2. Impact of grain size distribution on simulated SPM concentrations

451 During the May-June 2008 flood event, one can expect different sources of  
452 SPM for the three distinct periods described in section 2.2, with dam flushing  
453 operation during the 1st and the 3rd periods and natural floods during the 2nd  
454 period. As a consequence, one can expect different GSD for each of these pe-  
455 riods. As the GSD of SPM transported by the Isère River were not measured  
456 in 2008, simulation tests were run using the three hypothetical mixtures de-  
457 fined in Tab. 2 from samples collected in the Isère River during other events  
458 (Section 3.3). Results from these three simulations are presented in Fig. 6.

459 Simulated concentrations  $C_{\text{SPM}}$  obtained at Viviers station are compared  
460 with measured concentrations in Fig. 6. Simulated SPM concentrations are  
461 sensitive to grain size due to erosion/deposition and transport processes. Con-  
462 centrations  $C_{\text{SPM}}$  at Viviers using the coarse GSD (Mixture C) are half the  
463  $C_{\text{SPM}}$  simulated using the fine GSD (Mixture A). This is explained by the more  
464 intense deposition of the coarsest particles within the four hydropower schemes  
465 between the lowest Isère dam and Viviers.

466 For the flood period, although concentrations at Beaumont-Montoux were  
467 evaluated based on Viviers concentrations, the model yields an underestimation  
468 of the peak concentrations whatever the choice of GSD. This results from dis-  
469 persion processes. The concentration peak at Beaumont-Montoux should thus  
470 have been higher and narrower to take into account this effect. The difference  
471 between measured and simulated  $C_{\text{SPM}}$  could also be partly due to an overes-  
472 timation of the  $C_{\text{SPM}}$  measured at Viviers by the acoustic attenuation method,  
473 particularly when fine particles are highly concentrated, which increases the  
474 acoustic attenuation (Moore *et al.*, 2013).

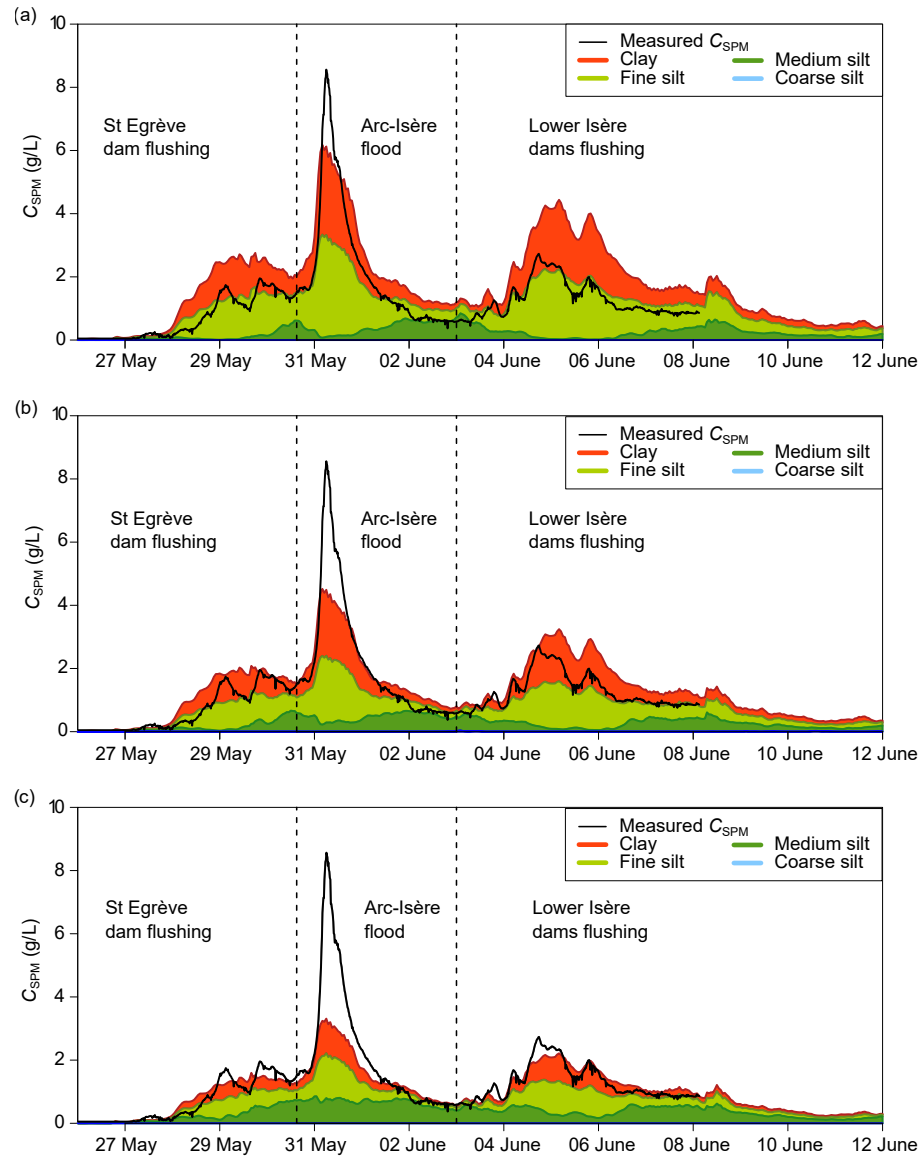


Figure 6: Simulated and measured SPM concentration ( $C_{SPM}$ ) at Viviers station for the three hypothetical GSD defined in Tab. 2: (a) Mixture A - Fine, (b) Mixture B - Medium and (c) Mixture C - Coarse.

475 Simulation tests also confirm that the GSD of the SPM transported was  
476 different during the three periods of the May-June 2008 flood event. During the



477 St Egrève Dam flushing period, the model using medium or coarse GSD (Mix-  
478 tures B or C) yields  $C_{SPM}$ -values in relatively good agreement with measured  
479 data. Mixture B was eventually preferred since it corresponds to measured data  
480 during the flood period of a similar event (in 2015). Also, it yields a better es-  
481 timation of peak concentrations. Flushing operation evacuated the coarse SPM  
482 from the St Egrève reservoir, but they were partially stored into the Lower Isère  
483 reservoirs, as the Lower Isère dams were operated with high water levels during  
484 this period. This could explain why the medium GSD is consistent with this  
485 situation.

486 During the Arc-Isère flood period, the  $C_{SPM}$  peak measured at Viviers  
487 reached about 9 g/L. Mixture A yielded the best agreement between simu-  
488 lated and measured  $C_{SPM}$  time series. Such very fine washload material, poorly  
489 represented in the bed, is brought from the Isère basin by the flood wave. Nev-  
490 ertheless, the simulated  $C_{SPM}$  peak reached only 6 g/L. As discussed above,  
491 the concentration peak at Beaumont-Montoux should have been higher and  
492 narrower. Using a finer GSD could also increase the simulated  $C_{SPM}$  peak.  
493 However, as discussed in section 3.3, a finer GSD would no longer correspond  
494 to the samples measured in the Isère River during floods of the Arc River.

495 For the third period of the event, corresponding to the Lower Isère dams  
496 flushing, Mixture C yields  $C_{SPM}$  at Viviers station that are in best agreement  
497 with measurements. This is consistent with the opening of the dam gates and  
498 the resuspension of coarser particles previously settled in the reservoir.

499 According to these observations, the GSD was parametrized as follows for  
500 the simulation of the May-June 2008 flood event: the medium GSD of Mixture  
501 B for the first period, the fine GSD of Mixture A for the second period and the  
502 coarse GSD of Mixture C for the third period.

#### 503 *4.3. Interaction of SPM with hydropower schemes*

504 The objective of this section is to study the SPM dynamics in interaction  
505 of SPM with hydropower schemes between the lowest Isère dam and Viviers  
506 station (Fig. 1). Five additional simulations were carried out to study the de-

507 position/erosion processes occurring in each hydropower scheme of the reach.  
508 The first simulation was run without activating deposition/erosion within the  
509 entire river system. In the other four simulations, deposition/erosion was suc-  
510 cessively activated in the four hydropower schemes of the system, which led to  
511 the decrease of the  $C_{SPM}$  simulated at Viviers (Fig. 7). Simulation of deposition  
512 is necessary to reproduce the  $C_{SPM}$  measured at Viviers. The simulated  $C_{SPM}$   
513 peak decreased from 4 to 2 g/L, 9 to 6 g/L, and 8 to 2 g/L in the first, second,  
514 and third period, respectively. This confirms that hydropower schemes are an  
515 obstacle to SPM transport due to the decreased flow velocity in dam reservoirs,  
516 which enhances deposition particularly for coarse SPM. Deposition is particu-  
517 larly intense during the dam flushing periods (first and third periods), as coarser  
518 GSD was parameterized for these periods (see section 4.2). These simulations  
519 also suggest that the largest decrease of  $C_{SPM}$  occurred in the Bourg-lès-Valence  
520 (BLV) scheme, between the lowest Isère dam and BLV dam. SPM also settled  
521 down within the next three hydro-electric schemes, but to a lesser extent since  
522 most of the coarsest particles settled down in the first scheme.

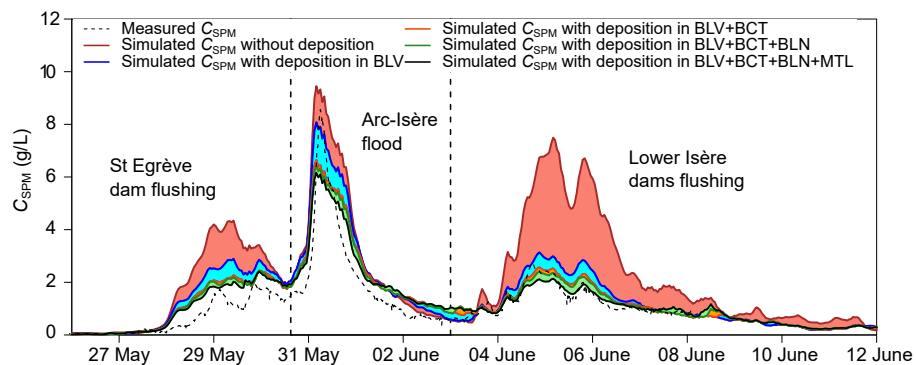


Figure 7: Measured and simulated SPM concentration ( $C_{SPM}$ ) at Viviers station during the May-June 2008 flood event, with deposition/erosion processes successively activated in the four hydropower schemes located between the lowest Isère dam and Viviers. BLV = Bourg-lès-Valence, BCT = Beauchastel, BLN = Baix-Le Logis Neuf, MTL = Montélimar. Coloured areas represent the cumulative SPM trapped in successive reservoirs.

523 The numerical model provides detailed information on the quantity and grain

524 size distribution of the SPM present in each branch of the river system at any  
525 time of the simulation. In order to better understand the deposition processes  
526 between the lowest Isère dam and the BLV dam observed in Fig. 7, the cumu-  
527 lative amounts of SPM settled in the area are presented in Fig. 8. At the scale  
528 of the entire event, the Isère River produced a total amount of 7.7 Mt of SPM,  
529 of which 2.8 Mt deposited at the Isère-Rhône confluence (Fig. 8d). The SPM  
530 deposition occurred mainly within three branches of the network: 60% in the  
531 lowest Isère branch, and 30% in the BLV and Beauchastel (BCT) power canals.  
532 Deposition mainly occurred during the second and third periods with a segre-  
533 gation in the grain size of the particle deposited, as also observed by *Camenen*  
534 *et al.* (2019). The Isère River produced 2.8 Mt during the second period, and  
535 80 % of this input, mainly composed of fine SPM, travelled through the BLV  
536 and BCT schemes. The remaining 20%, mainly composed of class 3 particles,  
537 were trapped in the BCT and BLV power canals, and not in the lowest Isère  
538 branch. But most of the deposition occurred during the third period when the  
539 Lower Isère dams were flushed. The SPM flux during this period was 3.8 Mt, i.e.  
540 half of the total input of the Isère during the event. SPM of class 4 represented  
541 30 % of the Isère River input, and these particles massively deposited within  
542 the Isère branch, and to a lesser extent within the BLV and BCT power canals.  
543 The deposits simulated in the downstream Isère reach are mainly composed of  
544 classes 3 and 4, which is consistent with available observations and with the  
545 choice of Mixture C as a coarse GSD representative of a deposit collected after  
546 the May 2015 flood.

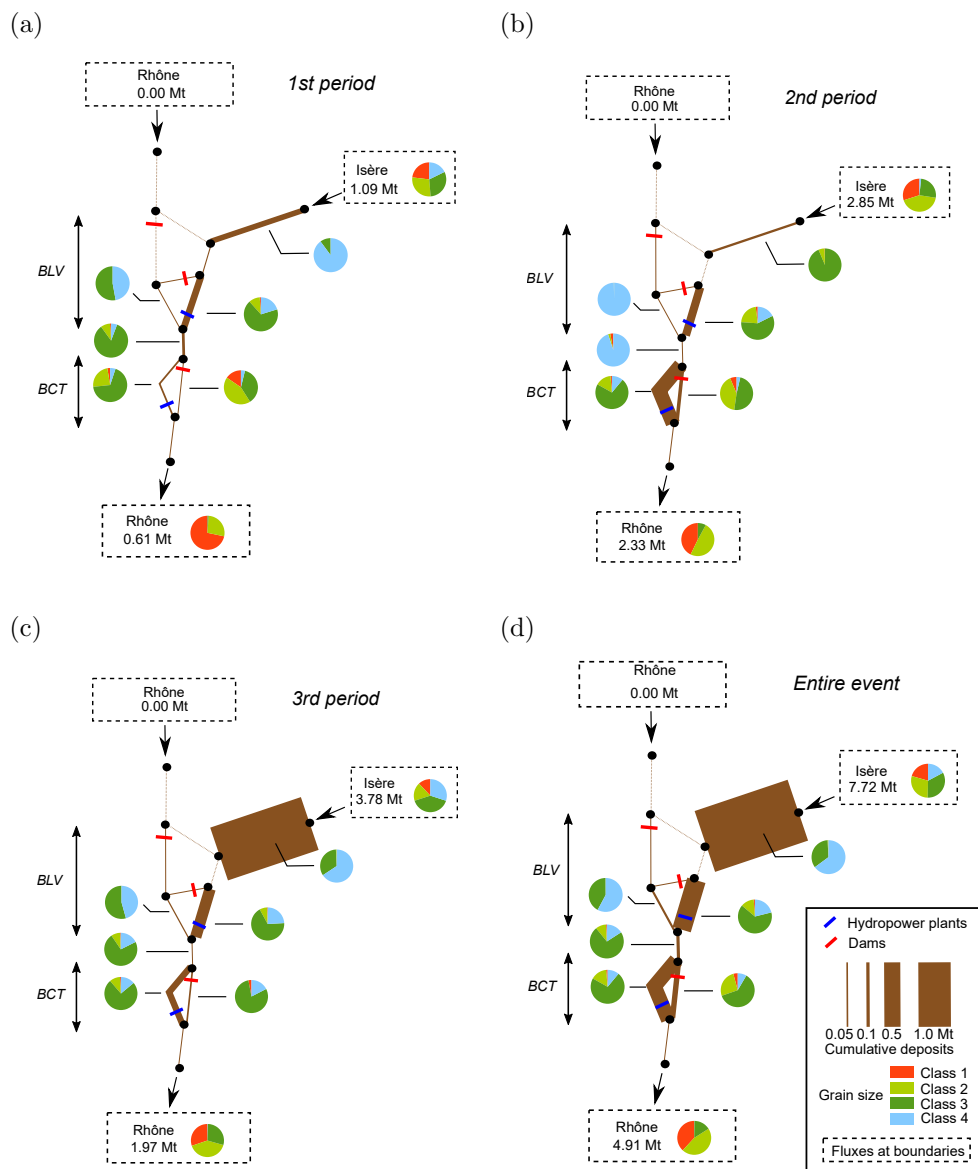


Figure 8: Mass and grain size composition of SPM deposited in the Isère-Rhône confluence system during the May-June 2008 flood event: first period (a), second period (b), third period (c) and entire event (d). See section 2.2 for definition of periods and Tab.2 for definition of grain size classes. The mass and grain size composition of SPM fluxes at boundaries are also shown. The thickness of the lines is proportional to the mass of SPM deposited in each reach. BLV = Bourg-lès-Valence scheme and BCT = Beauchastel scheme.

547 *4.4. Cumulative SPM fluxes*

548 Measured and simulated SPM cumulative fluxes are presented in Tab. 3 and  
549 Fig. 9 for the three periods (see section 2.2) and for the entire May-June 2008  
550 flood event at the monitoring stations in the Rhône River. In Fig. 9, the left-  
551 hand graphs display the cumulative fluxes estimated from observations whereas  
552 the right-hand graphs display the cumulative fluxes specified or simulated in the  
553 numerical model.

554 The relative deviation between the simulated and measured SPM cumulative  
555 fluxes was between +15 % and +36 % (see Tab. 3), except for the first period for  
556 which larger values are observed since measured cumulative fluxes are small. At  
557 Viviers station, the absolute deviation was around +0.8 Mt for the entire event  
558 for a total measured SPM flux of 3.6 Mt at this station. This relatively small  
559 deviation validates the reconstruction of the  $C_{\text{SPM}}$  time series at Beaumont-  
560 Monteux described in section 2.3, and the choice of the varying GSD for the  
561 three periods (see section 4.2). At Arles station, the measured SPM flux for the  
562 entire event was 4.2 Mt, and the simulated SPM flux was 5.7 Mt. *Eyrolle et al.*  
563 (2012) estimated this flux to be 4.7 Mt  $\pm$  30 %. These results are of the same  
564 order of magnitude and confirm the exceptional nature of the May-June 2008  
565 flood event.

566 As for the Durance River, the model highlighted the weakness of the hy-  
567 pothesis made of a very fine grain size distribution for the entire event. During  
568 the first week of the event, the relative deviation between measured and simu-  
569 lated fluxes increased from +50% to +133% between Viviers and Beaucaire (see  
570 Tab. 3). This is explained by the transfer of the SPM of the Durance directly  
571 to Beaucaire without deposition because of a too fine grain size distribution as-  
572 sumed for the Durance River SPM input during this first period. The measured  
573 SPM flux of 0.5 Mt only at Beaucaire during the first week indicated a large de-  
574 position of around 1.0 Mt at the Durance confluence. For the second and third  
575 periods, the hypothesis of a fine GSD for the Durance SPM input appeared  
576 more realistic although still a little bit too fine as the measured and simulated  
577 fluxes at Beaucaire were in better agreement. The fine SPM coming from the

Table 3: Measured and simulated SPM cumulative fluxes for the three periods (see section 2.2) and for the entire May-June 2008 flood event at the monitoring stations in the Rhône River, and relative deviations (RD) of the simulated fluxes to the measured flux.

	Rhône at Viviers			Rhône at Beaucaire			Rhône at Arles		
	Meas.	Model	RD	Meas.	Model	RD	Meas.	Model	RD
	Mt	Mt	%	Mt	Mt	%	Mt	Mt	%
Period 1	0.4	0.6	+50	0.6	1.4	+133	0.5	1.2	+140
Period 2	1.9	2.2	+16	2.6	3.0	+15	2.2	2.6	+18
Period 3	1.3	1.6	+23	1.7	2.1	+24	1.5	1.9	+27
Total	3.6	4.4	+22	4.9	6.5	+33	4.2	5.7	+36

578 Durance River during these two periods seemed to have travelled through the  
 579 downstream Durance reach and Rhône River down to the Delta with limited  
 580 deposition. For the downstream Durance reach, this also could be explained  
 581 during the second period because of the much higher discharges and velocities.

582 The model was also useful for estimating the amount of SPM transported  
 583 in the Petit Rhône at Fourques, where no  $C_{SPM}$  measurement were available.  
 584 The SPM flux of the Petit Rhône represented from 10 to 15 % of the SPM  
 585 fluxes measured at Beaucaire station. This is in good agreement with the water  
 586 discharge distribution between the Petit Rhône and the Grand Rhône observed  
 587 in long-term discharge time series (source CNR).

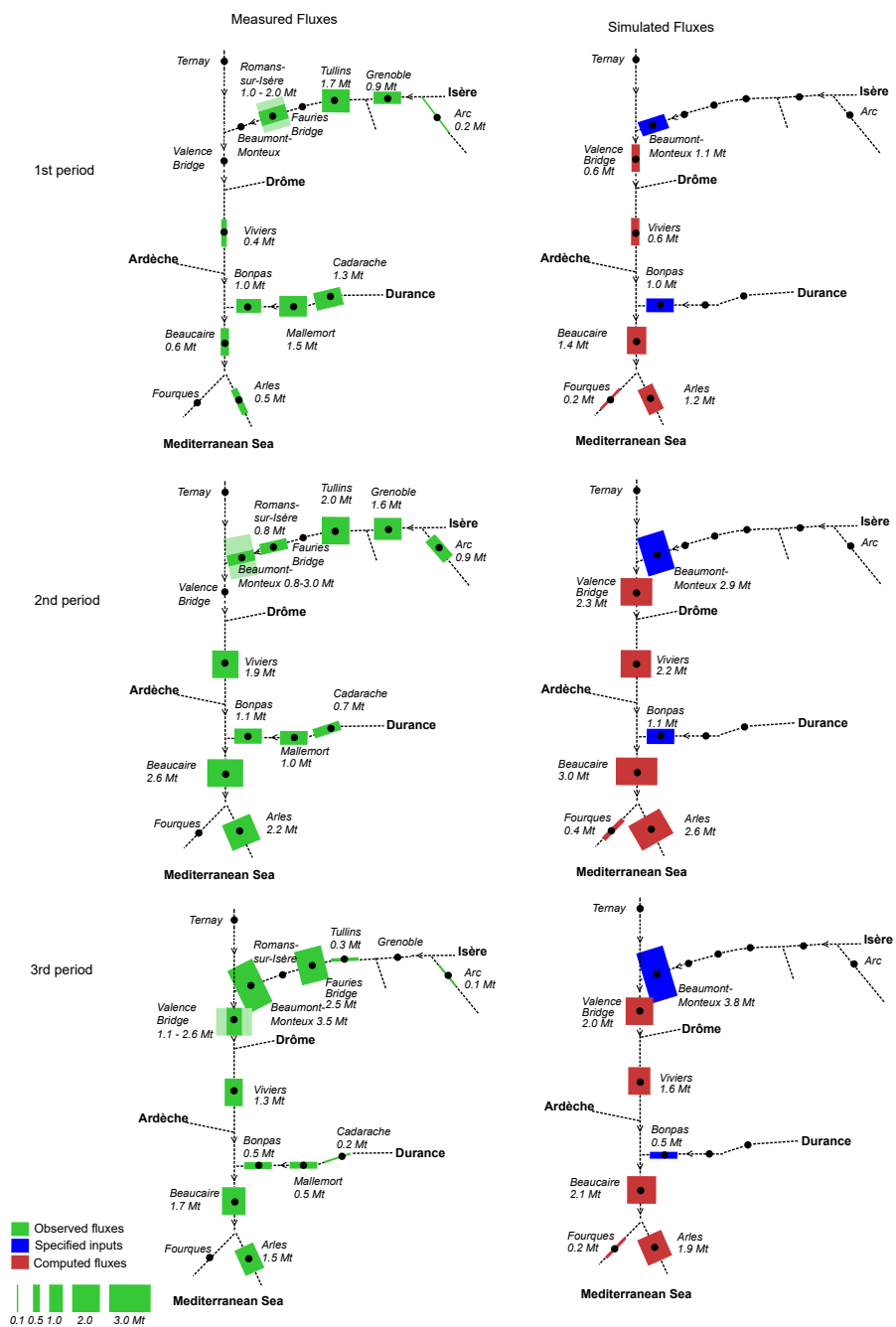


Figure 9: Monitored and simulated SPM cumulative fluxes (in Mt) along the Rhône River during the first, second and third periods of the 2008 flood event. Line thickness is proportional to SPM flux at the corresponding station.

588 4.5. Origin of the SPM

589 The origin of the SPM transported during the three periods of the event  
590 and measured at Arles was clarified. In particular, the Isère River input that  
591 was not measured during the first period could be quantified with the model.  
592 Fig. 10 shows the evolution of the measured and simulated  $C_{SPM}$  at Arles and  
593 the proportion of SPM coming from both the Isère and the Durance Rivers.  
594 The simulated  $C_{SPM}$  are close to the measured  $C_{SPM}$ , except the  $C_{SPM}$  peak  
595 recorded on 01/06/2008. The maximum recorded  $C_{SPM}$  was about 5 g/L while  
596 the maximum simulated  $C_{SPM}$  was 4 g/L, being a difference of 20 %. Fig. 10  
597 highlights the high contribution of the Durance River during the first days of  
598 the event, and the increasing contribution of the Isère River during the rest of  
599 the event. Approximately 50 % of the SPM fluxes came from the Durance River  
600 and the remaining 50 % came from the Isère River. Marion *et al.* (2010) and  
601 Eyrolle *et al.* (2012) discussed the origin of the SPM transited and deposited  
602 in the Grand-Rhône pro-delta during the May-June 2008 event. They assumed  
603 that most of the SPM came from the Durance River, therefore they investigated  
604 the origin of the SPM within the Durance river basin and ignored the equally  
605 large contribution of the Isère River.

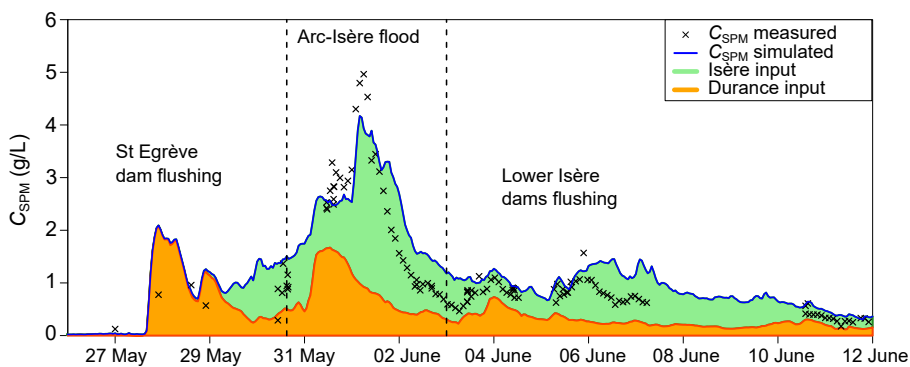


Figure 10: Simulated and measured  $C_{SPM}$  in the Rhône at Arles during the May-June 2008 flood event with decomposition of the Isère and Durance Rivers SPM inputs.

606 Nearly 50 % of the SPM flux brought by the Isère River to the Rhône



607 River system deposited in the river network before reaching Viviers. Although  
608 the model confirmed that the Rhône reservoirs acted as sediment sinks during  
609 the May-June 2008 flood event, they can turn to act as sediment sources due to  
610 resuspension during other floods. In the annual SPM fluxes computed by *Poulier*  
611 *et al.* (2019), there is evidence that the SPM deposited and stored during the  
612 2008 event were later re-suspended and exported during floods.

## 613 **5. Conclusive comments**

614 This paper explores the potential of numerical simulation to predict the  
615 sources and fate of SPM in regulated river networks. The main questions on  
616 numerical simulation tools addressed through this case study were: What is  
617 the added value of 1-D modelling of SPM fluxes? What are the most sensitive  
618 parameters? What are the main limitations and perspectives for improvement?

619 A 1-D hydrodynamical model was built and applied to a major hydro-  
620 sedimentary event in May-June 2008 in the Lower Rhône River, France. Such  
621 model would be the simplest and fastest possible hydrodynamical model that  
622 could be constructed and some physical processes that may be important are  
623 neglected in exchange for that simplicity. The Rhône River has a complex river  
624 network with confluences, bifurcations and hydropower schemes. The simula-  
625 tion code (AdisTS) was able to model the SPM fluxes at a high spatial and  
626 temporal resolution, which is useful to understand the SPM dynamics over the  
627 whole river system on time scales ranging from hour to decades, thanks to fast  
628 computational times. Especially, SPM supplies from the main tributaries and  
629 deposition of the coarsest particles behind hydropower structures could be quan-  
630 tified precisely, at any time and at any cross-section of the river network. The  
631 model provides insights that are not available from observational data alone. Es-  
632 pecially, the model simulates the continuous dynamics and spatial distribution  
633 of deposits, which would have allowed a better anticipation and management of  
634 sedimentation in critical areas of the Rhône reservoirs.

635 In the presented study case, approximately half of the 4.9 Mt of SPM mea-

636 sured at the outlet of the Rhône River catchment during the event were found  
637 to come from the Isère River and the other half from the Durance River whereas  
638 previous studies estimated that most of the flux at the outlet came from the  
639 Durance River. Also, the model confirmed that a large amount of the SPM de-  
640 livered by the Isère River was trapped behind the first hydro-electric scheme in  
641 the Rhône River, a cause of conflicts between dam operators. The high temporal  
642 and spatial resolution of fluxes computation is highly valuable for reconstruct-  
643 ing past events and also for managing future events like natural floods or dam  
644 flushing operations, by testing multiple dam operation scenarios. If forecasts  
645 of water discharges and SPM inputs are available, such a model can be used  
646 to compute real-time forecasts of SPM concentrations, fluxes and deposition  
647 throughout the river network.

648 As a basis for hydraulic simulation, an accurate description of the channel  
649 geometry and of the artificial structures is necessary, along with a conventional  
650 calibration of the friction coefficients along the river stretches. This was easily  
651 achieved in our case study. As for SPM simulation, the quality of the numeri-  
652 cal results was found to be highly sensitive to suspended sediment parameters,  
653 especially grain size, and to the operational rules of artificial structures. This  
654 may lead to substantial errors because accurate information on grain size distri-  
655 bution is often difficult to obtain, grain size varies spatially and temporally, and  
656 the coarsest particles may not be homogeneously distributed throughout the  
657 river cross-section. In this study, sensitivity tests made on the grain size dis-  
658 tribution of the SPM improved our knowledge of the Isère River input, despite  
659 the lack of measurements. Finer SPM particles were mostly transported during  
660 the natural flood period while coarser SPM were transported during the dam  
661 flushing periods. The simulation of deposition and erosion processes within the  
662 hydropower schemes was necessary to reproduce the strong deposition of SPM  
663 at the Isère confluence and further downstream. Deposits were mainly com-  
664 posed of the coarsest SPM (cf. *Camenen et al.*, 2019), while finer SPM travelled  
665 through the hydropower schemes without settling down.

666 Of course, observation and modelling supplement each other: dense and

667 precise SPM observational data measured at key points of the river system  
668 are necessary to specify the boundary conditions of numerical models, and to  
669 calibrate and validate them. An extended sensitivity analysis could be done  
670 to better infer upstream sediment supply, i.e. input concentrations and GSD.  
671 In the present paper, we constrained the tests to prior knowledge based on  
672 actual measurements and uncertainties. Another perspective of this work is to  
673 compare 1-D numerical modelling with chemical fingerprinting for quantifying  
674 SPM sources in the Rhône River for various hydrological conditions.

675 The 1-D numerical model applied in this study is typical of modern simu-  
676 lation tools used in river engineering applications. While the principles of 1-D  
677 hydrodynamical codes have virtually not changed for fifty years or so, their  
678 computation performance and the power of the available computers have been  
679 greatly improved. Compared to 2-D or 3-D hydrodynamical codes, 1-D hydro-  
680 dynamical codes offer much faster computational times allowing for real-time  
681 or long-term simulations and uncertainty analysis through Monte Carlo sim-  
682 ulation or sensitivity analysis (*Souhar and Faure, 2009*), which is practically  
683 challenging with higher level codes. The spatial resolution of 1-D hydrodynam-  
684 ical codes is sufficient for studying SPM dynamics on the river network scale,  
685 while 2-D or 3-D hydrodynamical codes would be required for studying local  
686 processes, in the close vicinity of artificial structures for instance. However, most  
687 1-D hydrodynamical codes still come with restrictive assumptions that call to be  
688 improved through future research. Computing the flow and suspended sediment  
689 flux interactions between the main channel and the floodways, or floodplains,  
690 is still motivating active research. More generally, the spanwise distribution of  
691 velocities, SPM concentrations and deposition/erosion fluxes throughout cross-  
692 sections has to be predicted from 1-D, i.e. cross-sectional average results. A  
693 major limitation of 1-D hydrodynamical codes is the usual assumption of full,  
694 instantaneous mixing of water and SPM downstream of confluences. In the case  
695 of the Rhône River, full mixing after a confluence is actually seldom reached  
696 before the next bifurcation between the navigation canal and the by-passed  
697 channel of the Old Rhône. Formulas for predicting the degree of mixing and the

698 spanwise distribution of SPM concentrations still have to be elaborated, based  
699 on tracing experiments conducted in the laboratory and in the field.

## 700 **Acknowledgments**

701 This study was conducted within the Rhône Sediment Observatory (OSR),  
702 a multi-partner research program funded through the Plan Rhône by the Euro-  
703 pean Regional Development Fund (ERDF), Agence de l'eau RMC, CNR, EDF  
704 and three regional councils (Auvergne-Rhône-Alpes, PACA and Occitanie). The  
705 PhD scholarship of Marina Launay (2010-2014) was funded by the Rhône-Alpes  
706 regional council. Authors also thank many collaborators at Irstea, Cerege,  
707 IRSN, MIO and Ifremer for their contributions to the field work and the chem-  
708 ical analyses. This work builds on the developments of earlier versions of the  
709 1-D Rhône model achieved by Emilie Andriès and Carla Walter (Irstea).

## 710 **References**

- 711 AFNOR (2005), NF EN 872 : Water quality - Determination of suspended  
712 solids - Method by filtration through glass fibre filters (in French), 10 p.
- 713 Armanini, A., and G. Di Silvio (1988), A one-dimensional model for the trans-  
714 port of a sediment mixture in non-equilibrium conditions, *26(3)*, 275–292,  
715 doi:10.1080/00221688809499212.
- 716 Camenen, B. (2007), Simple and general formula for the settling velocity of  
717 particles, *Journal of Hydraulic Engineering-ASCE*, *133*, 229–233, doi:10.1061/  
718 (ASCE)0733-9429(2007)133:2(229).
- 719 Camenen, B., E. Perret, A. Herrero, C. Berni, F. Thollet, A. Buffet, G. Dramais,  
720 C. Le Bescond, and M. Lagouy (2016), Estimation of the volume of a fine  
721 sediment deposit over a gravel bar during a flushing event, in *River Flow*  
722 *2016*, *CRC Press*, pp. 533–540.

- 723 Camenen, B., G. Naudet, G. Dramais, J. Le Coz, and A. Paquier (2019) A multi-  
724 technique approach for evaluating sand dynamics in a complex engineered  
725 piedmont river system, *Science of the Total Environment*, 657, 485—497, doi:  
726 10.1016/j.scitotenv.2018.11.394.
- 727 Clifford, N., K. Richards, R. Brown, and S. Lane (1995), Laboratory and field  
728 assessment of an infrared turbidity probe and its response to particle-size and  
729 variation in suspended sediment concentration, *Hydrological Sciences Journal*,  
730 40(6), 771–791, doi:10.1080/02626669509491464.
- 731 Copard, Y., F. Eyrolle, O. Radakovitch, A. Poirel, P. Raimbault, S. Gairoard,  
732 and C. Di-Giovanni (2018) Badlands as a hot spot of petrogenic contribution  
733 to riverine particulate organic carbon to the Gulf of Lion (NW Mediterranean  
734 Sea), *Earth Surface Processes and Landforms*, in press, doi:10.1002/esp.4409
- 735 Druine, F., R. Verney, J. Deloffre, J.P. Lemoine, M. Chapalain, V. Landemaine,  
736 and R. Lafite (2018), In situ high frequency long term measurements of sus-  
737 pended sediment concentration in turbid estuarine system (Seine Estuary,  
738 France): Optical turbidity sensors response to suspended sediment character-  
739 istics, *Marine Geology*, 400, 24–37
- 740 Dugué, V., C. Walter, E. Andries, M. Launay, J. Le Coz, B. Camenen, and  
741 J.-B. Faure (2015), Accounting for hydropower schemes' operation rules in  
742 the 1D hydrodynamic modeling of the Rhône River from Lake Geneva to the  
743 Mediterranean Sea, in *E-proceedings of the 36th IAHR World Congress*, 28  
744 June - 3 July, 2015, *The Hague, The Netherlands*, p. 9.
- 745 El Kadi Abderrezzak, K., and A. Paquier (2009), One-dimensional numerical  
746 modeling of sediment transport and bed deformation in open channels, *Water*  
747 *Resources Research*, 45(5), doi:10.1029/2008{WR}007134, W05404.
- 748 Eyrolle, F., O. Radakovitch, and P. Raimbault (2012), Consequences of hydro-  
749 logical events on the delivery of suspended sediment and associated radionu-  
750 clides from the Rhône River to the Mediterranean Sea, *Journal of Soils and*  
751 *Sediments*, 12, 1479–1495, doi:10.1007/s11368-012-0575-0.

- 752 Foster, I., R. Millington, and R. Grew (1992), The impact of particle size  
753 controls on stream turbidity measurement; some implications for suspended  
754 sediment yield estimation, *Erosion and sediment transport monitoring pro-  
755 grammes in river basins*, 210, 51–62.
- 756 Garneau, C., S. Sauvage, A. Probst, and J. Sánchez-Pérez (2015), Mod-  
757 elling of trace metal transfer in a large river under different hydrological  
758 conditions (the Garonne River in southwest France), *Ecological Modelling*,  
759 306(Supplement C), 195 – 204, doi:[https://doi.org/10.1016/j.ecolmodel.2014.  
760 09.011](https://doi.org/10.1016/j.ecolmodel.2014.09.011).
- 761 Gippel, C. (1995), Potential of turbidity monitoring for measuring the transport  
762 of suspended-solids in streams, *Hydrological Processes*, 9(1), 83–97, doi:10.  
763 1002/hyp.3360090108.
- 764 Gray, J. and J. Gartner (2010)., Technological advances in suspended-sediment  
765 surrogate monitoring, *Water Resources Research*, 46(4):W00D29
- 766 Guertault, L. (2015), Evaluation of the hydro-sedimentary processes of an elon-  
767 gated dam reservoir: Application to the Génissiat reservoir located on the  
768 Upper-Rhône River (in French), PhD, Université Claude Bernard Lyon 1,  
769 Lyon, France, 239 p.
- 770 Guertault, L., B. Camenen, C. Peteuil, A. Paquier, and J.-B. Faure (2016), One-  
771 Dimensional Modeling of Suspended Sediment Dynamics in Dam Reservoirs,  
772 *Journal of Hydraulic Engineering-ASCE*, 142(10), doi:10.1061/(ASCE)  
773 }{HY}.1943-7900.0001157.
- 774 Han, Q. (1980), A study on the non-equilibrium transportation of suspended  
775 load, in *1st Int. Symp. on River Sedimentation*, *Chinese Society of Hydraulic  
776 Engineering, China*, pp. 793–802.
- 777 Horner I., B. Renard, J. Le Coz, F. Branger, H.K. McMillan, and G. Pierrefeu  
778 (2018), Impact of stage measurement errors on streamflow uncertainty, *Water  
779 Resources Research*, 54, 1952–1976.

- 780 Horowitz, A. (2008), Determining annual suspended sediment and sediment-  
781 associated trace element and nutrient fluxes, *Science of the Total Environ-*  
782 *ment*, 400(1-3), 315–343, doi:10.1016/j.scitotenv.2008.04.022.
- 783 Horowitz, A., K. Elrick, and J. Smith (2001), Estimating suspended sediment  
784 and trace element fluxes in large river basins: methodological considerations  
785 as applied to the NASQAN programme, *Hydrological Processes*, 15(7), 1107–  
786 1132, doi:10.1002/hyp.206.
- 787 Horowitz, A. J., R. T. Clarke, and G. H. Merten (2015), The effects of sample  
788 scheduling and sample numbers on estimates of the annual fluxes of suspended  
789 sediment in fluvial systems, *Hydrological Processes*, 29(4), 531–543, doi:10.  
790 1002/hyp.10172.
- 791 Iwasa, Y., and S. Aya (1991), Predicting longitudinal dispersion coefficient in  
792 open channel flows, in *Int. Symp. on Environmental Hydraulics*, IAHR, Hong-  
793 Kong, China, pp. 505–510.
- 794 Kondolf, G.M., Y. Gao, G.W. Annandale, G.L. Morris, E. Jiang, J. Zhang,  
795 Y. Cao, P. Carling, K. Fu, Q. Guo, R. Hotchkiss, C. Peteuil, T. Sumi, H.-  
796 W. Wang, Z. Wang, Z. Wei, B. Wu, C. Wu, and C.T. Yang (2015), Sustain-  
797 able sediment management in reservoirs and regulated rivers: Experiences  
798 from five continents, *Earth'Future*, 2, 1 – 25, doi:http://dx.doi.org/10.1002/  
799 2013EF000184.
- 800 Krone, R. (1962), Flume studies of the transport of sediment in estuarial shoal-  
801 ing processes: final report, *Tech. rep.*, Hydraulic Eng. Lab. and Sanitary Eng.  
802 Res. Lab., University of California, Berkeley, California, USA, 110 p.
- 803 Launay, M. (2014), Fluxes of suspended particulate matters, particulate mer-  
804 cury and PCBs in the Rhône River, from Lake Geneva to the Mediterranean  
805 Sea (in French), PhD, Claude Bernard University Lyon 1, Lyon, France,  
806 432 p.

- 807 Launay, M., J. Le Coz, B. Camenen, C. Walter, H. Angot, G. Dramais, J.-  
808 B. Faure, and M. Coquery (2015), Calibrating pollutant dispersion in 1-D  
809 hydraulic models of river networks, *Journal of Hydro-Environment Research*,  
810 9(1), 120 – 132, doi:<http://dx.doi.org/10.1016/j.jher.2014.07.005>.
- 811 Legout, C., I.A. Droppo, J. Coutaz, C. Bel, and M. Jodeau (2018), Assess-  
812 ment of erosion and settling properties of fine sediments stored in cob-  
813 ble bed rivers: the Arc and Isère alpine rivers before and after reservoir  
814 flushing, *Earth Surface Processes and Landforms*, 43(6), 1295 – 1309, doi:  
815 <http://dx.doi.org/10.1002/esp.4314>.
- 816 Ludwig, W., E. Dumont, M. Meybeck, and S. Heussner (2009), River discharges  
817 of water and nutrients to the Mediterranean and Black Sea: Major drivers for  
818 ecosystem changes during past and future decades? *Progress in Oceanography*,  
819 80(3-4), 199 – 217, doi:<https://doi.org/10.1016/j.pocean.2009.02.001>.
- 820 Mano, V., J. Nemery, P. Belleudy, and A. Poirel (2008), One year of suspended  
821 particle matter (SPM) and carbon fluxes on an alpine river : the Isere River  
822 (in French), *La Houille Blanche*, (5), 64 p.
- 823 Marion, C., G. Maillet, M. Arnaud, and F. Eyrolle (2010), Quantification of the  
824 Rhône solid fluxes at the mouth: contributions of the Durance River during  
825 the exceptional flood of May 2008 (in French), *La Houille Blanche*, (5), 72–80,  
826 doi:10.1051/lhb/2010057.
- 827 Masson, M., H. Angot, C. Le Bescond, M. Launay, A. Dabrin, C. Miège, J. Le  
828 Coz, and M. Coquery (2018), Sampling of suspended particulate matter using  
829 particle traps in the Rhône River: Relevance and representativeness for the  
830 monitoring of contaminants, *Science of the Total Environment*, 637–638, 538–  
831 549, doi:10.1016/j.scitotenv.2018.04.343.
- 832 Moatar, F., M. Meybeck, S. Raymond, A. Coynel, W. Ludwig, V. Mano, J. Ne-  
833 mery, A. Poirel, H. Etcheber, and P. Crouzet (2008), SPM fluxes estimates  
834 from discrete monitoring: comparison of calculation methods and uncertaini-  
835 ties, *La Houille Blanche*, (4), 64–71.



- 836 Moore, S. A., J. Le Coz, D. Hurther, and A. Paquier (2012), On the Application  
837 of Horizontal ADCPs to Suspended Sediment Transport Surveys in Rivers,  
838 *Continental Shelf Research*, 46, 50–63.
- 839 Moore, S. A., J. Le Coz, D. Hurther, and A. Paquier (2013), Using multi-  
840 frequency acoustic attenuation to monitor grain size and concentration of  
841 suspended sediment in rivers, *Journal of the Acoustical Society of America*,  
842 133(4), 1959–1970, doi:{10.1121/1.4792645}.
- 843 Navratil, O., O. Evrard, M. Esteves, C. Legout, S. Ayrault, J. Nemery, A. Mate  
844 Marin, M. Ahmadi, I. Lefevre, A. Poirel, and P. Bonte (2012), Temporal  
845 variability of suspended sediment sources in an alpine catchment combining  
846 river/rainfall monitoring and sediment fingerprinting, *Earth Surface Processes  
847 and Landforms*, 37(8), 828–846, doi:10.1002/esp.3201.
- 848 Nicollet, G., and M. Uan (1979), Permanent flows with free surface in com-  
849 pounds beds (in French), *La Houille Blanche*, 1, 21–30.
- 850 Ollivier, P., B. Hamelin, and O. Radakovitch (2010), Seasonal variations of phys-  
851 ical and chemical erosion: A three-years survey of the Rhone river (France),  
852 *Geochimica et Cosmochimica Acta*, 74(no 3), 907–927.
- 853 Papanicolaou, A. T. N., M. Elhakeem, G. Krallis, S. Prakash, and J. Edinger  
854 (2008), Sediment Transport Modeling Review: Current and Future De-  
855 velopments, *Journal of Hydraulic Engineering-ASCE*, 134(1), 1–14, doi:  
856 10.1061/({ASCE})0733-9429(2008)134:1(1).
- 857 Pardé, M. (1925), *The hydrological regime of the Rhône River (in French)*.  
858 *Institut de Géographie Alpine*, vol. 13:3, 459–547 pp.
- 859 Partheniades, E. (1965), Erosion and deposition of cohesive soils, *Journal of  
860 Hydraulic Division*, 91, 105–139.
- 861 Phillips, J., B. Webb, D. Walling, and G. Leeks (1999), Estimating the sus-  
862 pended sediment loads of rivers in the LOIS study area using infrequent sam-  
863 ples, *Hydrological Processes*, 13(7), 1035–1050.

- 864 Pont, D. (1997), The discharge of suspended sediments near to the mouth of  
865 the Rhône recent statistics (1994-1995) (in French), *Revue de Géographie de*  
866 *Lyon*, 72(1), 23–33, doi:10.3406/geoca.1997.4675.
- 867 Pont, D., J. Simonnet, and A. Walter (2002), Medium-term changes in sus-  
868 pended sediment delivery to the ocean: Consequences of catchment hetero-  
869 geneity and river management (Rhône River, France), *Estuarine Coastal and*  
870 *Shelf Science*, 54(1), 1–18, doi:10.1006/ecss.2001.0829.
- 871 Poulhier, G., M. Launay, C. Le Bescond, F. Thollet, M. Coquery, and J. Le Coz  
872 (2019), Combining flux monitoring and data reconstruction to establish an-  
873 nual budgets of suspended particulate matter, mercury and PCB in the Rhône  
874 River from Lake Geneva to the Mediterranean Sea, *Science of the Total En-*  
875 *vironment*, 658, 457–473, doi:10.1016/j.scitotenv.2018.12.075.
- 876 Radakovitch, O., V. Roussiez, P. Ollivier, W. Ludwig, C. Grenz, and J.-L.  
877 Probst (2008), Input of particulate heavy metals from rivers and associated  
878 sedimentary deposits on the Gulf of Lion continental shelf, *Estuarine, Coastal*  
879 *and Shelf Science*, 77(2), 285–295.
- 880 Rieux, C. (2008), Report of the Lower Isère dam flushing. Results of the physico-  
881 chemical monitoring from 2 to 12 of June 2008 (in French), *Tech. Rep.*  
882 *D4161/RAP/2008-00653-A*, EDF, 29 p.
- 883 Souhar, O., and J.-B. Faure (2009), Approach for uncertainty propagation and  
884 design in Saint-Venante equations via automatic sensitive derivatives applied  
885 to Saar river, *Canadian Journal of Civil Engineering*, 36(7), 1144–1154.
- 886 Thollet, F., J. Le Coz, G. Antoine, P. François, L. Saguintaah, M. Launay, and  
887 B. Camenen (2013), Influence of grain size changes on the turbidity mea-  
888 surement of suspended solid fluxes in watercourses (in French), *La Houille*  
889 *Blanche*, 4, 50–56.
- 890 Ulke, A., G. Tayfur, and S. Ozkul (2017), Investigating a suitable empirical  
891 model and performing regional analysis for the suspended sediment load pre-

- 892 diction in major rivers of the Aegean region, Turkey, *Water Resources Man-*  
893 *agement*, 31(3), 739–764, doi:10.1007/s11269-016-1357-z.
- 894 Walling, D., and B. Webb (1985), Estimating the discharge of contaminants  
895 to coastal waters by rivers - some cautionary comments, *Marine Pollution*  
896 *Bulletin*, 16(12), 488–492, doi:10.1016/0025-326{X}(85)90382-0.
- 897 Walling, D., P. Owens, J. Carter, G. Leeks, S. Lewis, A. Meharg, and J. Wright  
898 (2003), Storage of sediment-associated nutrients and contaminants in river  
899 channel and floodplain systems, *Applied Geochemistry*, 18(2), 195–220.
- 900 Wu, W., D. A. Vieira, and S. S. Y. Wang (2004), One-Dimensional Numerical  
901 Model for Nonuniform Sediment Transport under Unsteady Flows in Channel  
902 Networks, *Journal of Hydraulic Engineering-ASCE*, 130(9), 914–923, doi:10.  
903 1061/({ASCE})0733-9429(2004)130:9(914).